

Quasi unidimensional growth of Co nanostructures on a strained Au(111) surface

P. Campiglio^{a,b}, V. Repain^{a,*}, C. Chacon^a, O. Fruchart^c, J. Lagoute^a, Y. Girard^a, S. Rousset^a

^a Laboratoire Matériaux et Phénomènes Quantiques, Université Paris Diderot & CNRS, UMR 7162, case courrier 7021, F-75205 Paris Cedex 13, France

^b Department of Materials Science, Università degli Studi di Milano-Bicocca, Via R. Cozzi 53 Milano, 20125, Italy

^c Institut Néel, CNRS & Université Joseph Fourier, F-38042 Grenoble Cedex 9, France

ARTICLE INFO

Article history:

Received 4 January 2011

Accepted 24 March 2011

Available online 3 April 2011

Keywords:

Self-assembly

Surface diffusion

Low index single crystal surfaces

Metal-metal magnetic thin films structures

Scanning tunneling microscopy

Cobalt

ABSTRACT

We investigated to which extent a uniaxially-strained Au(111) surface, thereby displaying linear reconstructions, may be used as a template for the growth of elongated nanostructures. Cobalt has been used as a deposition material and two routes have been followed satisfactorily. The first one consists of the control of diffusion through the temperature of deposition. The second one consists of a first step of platinum seeding in the reconstruction, followed by cobalt deposition with nucleation on the platinum seeds.

© 2011 Elsevier B.V. All rights reserved.

1. Introduction

The ability to organize matter into objects with regular size, shape and spacing down to the atomic scale represents a cornerstone for nanoscience and nanotechnology. Top-down methods, mainly based on lithographic techniques, are time-consuming, expensive and in most cases limited to sizes above a few tens of nanometers. In this context a promising alternative relies on bottom-up approaches. These exploit diffusion and aggregation processes specific to each system, to drive the assembly of atoms and molecules in nanostructures [1]. Such routes are particularly interesting when using pre-existing self-organized template surfaces [2], which guide the growth and yield ordered arrays of nanodots. One major output of using surface templates is that the resulting nanostructures display a narrow size distribution. The guiding effect of the template may often be applied to several materials, which otherwise would not give rise to an organized array. For metal surfaces, a model template is provided by the Au(111) surface. It displays a so-called herringbone reconstruction [3] at the elbows of which many materials may nucleate and form ordered arrays of dots [4,5]. The distance between nearest-neighbor dots is about 7 nm, and the metallic clusters have a nearly mono-disperse lateral size up to a few nanometers in diameter. On the one hand this peculiarity has allowed the study of fundamental physical properties (notably the magnetic anisotropy) of low dimensional model systems [6–8]. On the other hand, the Au(111)

surface lacks versatility since its surface pattern makes it difficult to control the dots' shape. In particular, the natural surface of Au(111) does not allow the versatile growth of nanowires, because its template is two-dimensional with a rectangular unit cell. In fact local nanowires can be achieved for certain materials in a narrow range of coverage when coalescence sets in [9] but they are not macroscopically oriented along the same direction. So far, oriented nanowires have been grown on anisotropic substrates like (110) surface of fcc metals [10,11], vicinal surfaces [12], molecular networks [13] or ripples obtained by etching under kinetic limitations [14,15]. The interest concerning nanowires is due to their promising use as building blocks in electronics [16], photonics [17], sensoristics [18] and thermoelectrics [19]. The use of dense surfaces for the growth of nanowires would be a technological improvement since they are the most common surfaces observed during thin films growth. Au(111) appears to be a good candidate for anisotropic dense surface. Indeed, when subjected to a uniaxial strain, it has been shown that it may display a purely linear reconstruction, instead of the usual herringbone [20]. While initially performed *in situ* on a bent mica sheet, providing only a temporary control of the strain, recently linear reconstructions on Au(111) could be stabilized by uniaxial epitaxial strain on a body-centered cubic W(110) underlayer film [21]. Linear reconstruction has been observed also on Au(111)/mica, where dislocations locally alter the elastic field. In this case some evidences for anisotropic diffusion were found [22].

In this paper, we investigate to what extent this new Au(111) linear reconstruction may be used as a template for self-organizing wires or chains of dots. We successfully produced elongated-shaped nanodots of cobalt following two routes. The first one relies on the

* Corresponding author.

E-mail address: vincent.repain@univ-paris-diderot.fr (V. Repain).

temperature control over the diffusion of Co adatoms while the second one exploits the gold–platinum surface alloy to create a prepatterned surface with controlled nucleation sites.

2. Experimental details

The samples consist of an Au(111)/W(110) thin film epitaxially grown on sapphire ($11\bar{2}0$) by pulsed-laser deposition in a first ultra-high vacuum chamber. The base pressure is 3×10^{-11} mbar and the typical deposition rate is 1 ML(monolayer)/s [23]. The samples were transferred through air to another chamber for the STM studies. The base pressure is better than 10^{-10} mbar. Here the sample is cleaned with repeated cycles of grazing-incidence bombardment with argon ions (typically for 30 s with an incidence angle $\alpha = 45^\circ$ at an Ar pressure of 2×10^{-6} mbar and a voltage of 1 kV) followed by annealing at 920 K. Cobalt and platinum were evaporated by electron bombardment heating of high purity rods (99.99%). Typical flux rates are 0.2 ML/min and 0.02 ML/min for Co and Pt respectively. The deposition is performed on the sample placed in an Omicron Nanotechnology©VT-STM (operating range from 50 K to 500 K). The cobalt and platinum coverage (θ_{Co} and θ_{Pt}) are determined on the basis of STM images, assuming a pseudomorphic growth with the Au(111) substrate. The pressure during deposition is always maintained below 1×10^{-10} mbar. Morphological studies are made by *in situ* STM at the temperature of the deposition.

3. Results and discussion

3.1. Au(111) with unidirectional reconstruction

The driving force for Au(111) surface reconstruction is the surface tensile stress. In response to this the surface layer spontaneously densifies along the $\langle 1\bar{1}0 \rangle$ directions, adding one extra atom every 22 atoms of the underlying layer with bulk lattice parameters, giving rise to the $22 \times \sqrt{3}$ reconstruction [24,25]. Inside the unit cell the atoms are arranged in fcc and hcp-type stacking domains separated by two stacking fault lines (or discommensuration lines). At larger scale a so-called herringbone reconstruction is observed: the $22 \times \sqrt{3}$ domains bend of 120° and form a mesoscopically ordered pattern with a typical period of $a_1 = 7$ nm and $a_2 \approx 25$ nm (but can vary between 20 and 30 nm according to the area or the samples) [3,26]. This secondary superstructure arises from long-range elastic interactions mediated by the substrate, to relax a compression otherwise unidirectional [27]. Because of such central role played in the reconstruction, it is clear that stress is a key parameter to handle if one wishes to guide the surface towards new arrangements.

To this purpose we used a multilayer sample (schematically shown in Fig. 1) in which a uniaxial in-plane strain is imposed through the epitaxial relation with an underlayer with a crystalline uniaxial symmetry [21].

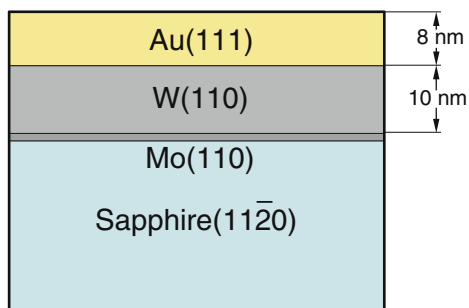


Fig. 1. Schematic structure of the multilayer sample employed. The thickness of the Mo layer is 0.7 nm.

In short, the substrate we chose for our sample is a sapphire ($11\bar{2}0$) surface, over which a very thin film (0.7 nm) of Mo and a thicker one (10 nm) of W are grown and annealed such as to yield a single-crystalline body-centered layer with an atomically-smooth surface, with terraces of several hundreds of nanometers in width [23]. Mo and W are bcc metals and they both expose the (110) surface during the growth. This terminal plan is characterized by a centered rectangular bidimensional lattice. Due to its anisotropy this layer induces a uniaxial strain in the Au layer (deposited at room temperature and annealed at 400°C), lifting the original three-fold symmetry and inducing a preferential orientation of the compressed $[1\bar{1}0]$ direction [21]. The initial thickness of the Au layer is 8 nm.

In Fig. 2a an image of the uniaxial Au(111) surface is reported. The brighter lines are the discommensuration lines that run along the $[11\bar{2}]$ direction, while in the close-packed $[1\bar{1}0]$ direction hcp and fcc atomic stacking regularly alternate. As can be clearly seen, the herringbone reconstruction is suppressed and the purely linear reconstruction is stable over the whole sample surface. The stacking fault lines are characterized by a corrugation height of 0.17 ± 0.02 Å while the distance between two adjacent maxima is close to 57 Å, in contrast to the value observed for the reconstruction of Au(111) single-crystal surface (64 Å). Indeed, the supercell that can be identified in Fig. 2b shows that the periodicity is equal to 20 atomic positions.

At larger scale (Fig. 3a) some defects of the reconstruction also appear, mainly due to surface morphology. The most visible signatures in STM images come from screw dislocations that appear as emerging steps. Edge dislocations leave weaker footprints on the morphology, but are responsible for important deviations from the purely linear reconstruction. At the surface, edge dislocations split into two partial dislocations that elastically repel each other and form a stacking fault ribbon that appears like a short step segment one-third of the full step height. These defects have been occasionally seen on single crystal Au(111) surfaces [28]. Stacking fault ribbons are

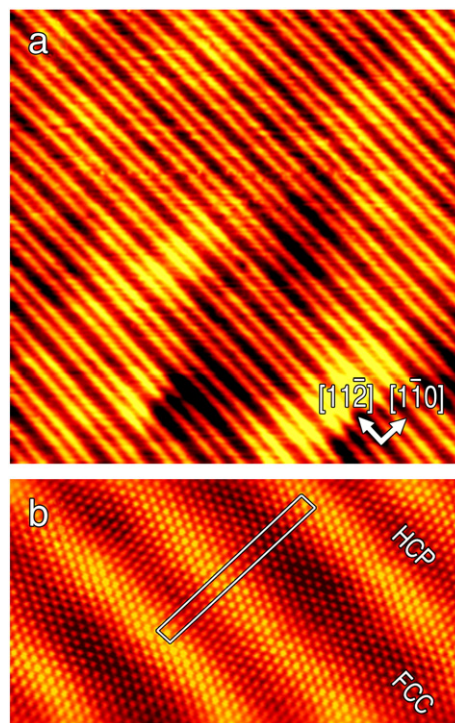


Fig. 2. (a) Room temperature STM image showing the unidirectional reconstruction of the stressed Au(111) surface (85×85 nm²). (b) Drift compensated atomic resolution STM image, with the unit cell highlighted (15×8 nm²). The size of the unit cell is 5×57 Å².

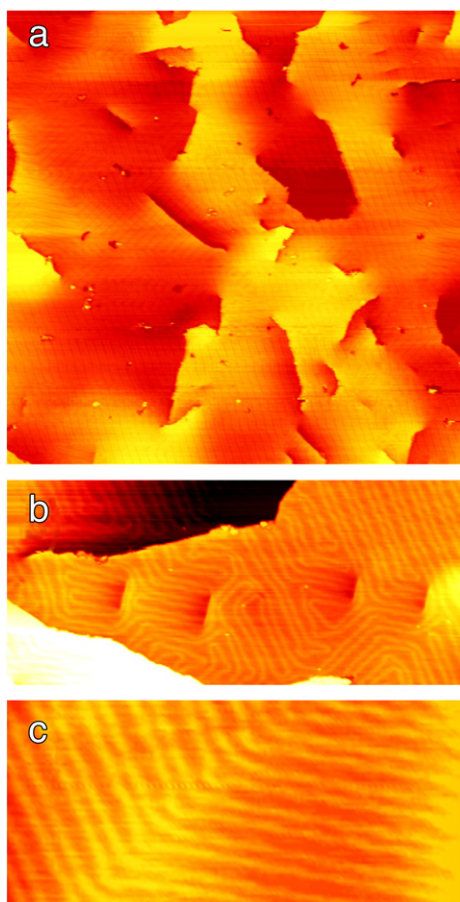


Fig. 3. STM images of the Au(111) thin film surface. (a) Large scale image of the surface ($360 \times 360 \text{ nm}^2$). (b) Effect of a sequence of stacking fault ribbons on Au(111) reconstruction ($130 \times 60 \text{ nm}^2$). (c) The reconstruction deviates from its unidimensional character and turns of 120° as in the herringbone reconstruction ($60 \times 30 \text{ nm}^2$).

commonly arranged in sequences, like shown in Fig. 3b, probably arising from grain boundaries. When the reconstruction deviates from its unidimensional character, it turns of 120° as in the herringbone reconstruction (Fig. 3c). The reconstruction elbows still constitute the main trap for adatoms and represent the principal difficulty to overcome in order to obtain a homogeneous growth. The density of defects may probably be decreased. Pathways for these should be based on the systematic investigation of parameters such as growth temperature or annealing, thickness of layer, and misfit with the buffer e.g. using solid solutions [29].

3.2. Growth of Co on Au(111)

Co was deposited at low coverage (θ_{Co}) in a wide range of temperatures ($50 \text{ K} < T < 300 \text{ K}$) on an Au(111) surface with unidirectional reconstruction. When the deposition of 0.25 ML of Co is carried out at room temperature the Co growth proceeds very differently compared to the growth on herringbone reconstruction (Fig. 4a) [30]. While the profile analysis indicates that the dots retain the usual bilayer height, the absence of periodic elbows in the reconstruction makes the dots lose both their regular spacing and their narrow size distribution (Fig. 4b). All the diffusion channels are clearly activated along all directions and thus the diffusion of adatoms is essentially isotropic. Due to the long diffusion length at this temperature, the adatoms are eventually pinned at defects of the surface.

As a consequence of the substrate anisotropy, Co adatoms are facing orientation dependent diffusion barriers with characteristic

activation energies [4]. This permits control of the diffusion channels only by changing the temperature of the substrate during deposition. To obtain an anisotropic diffusion on the Au(111) unidirectional reconstruction, we have reduced the temperature of the substrate to 105 K during Co deposition. The deposition temperature is not very critical, as the processes described below were found to be identical at 135 K. As can be seen in Fig. 4c, Co ($\theta_{\text{Co}} = 0.15 \text{ ML}$) forms dots elongated along the reconstruction direction, up to 20 nm long and with a mean aspect ratio equal to 5. The nucleation of this kind of dots takes place on the fcc zone of the reconstruction. From these observations we can deduce that at this temperature the diffusion is anisotropic, with the path of adatoms along a direction parallel to the discommensuration lines being favored. Thus, in this temperature range the discommensuration lines seem to act as an energy barrier, repelling the diffusion of Co adatoms as observed for Al [31]. Molecular dynamic simulations predicted a more favorable diffusion perpendicular to the discommensuration lines, which constitute a favored path to kink sites, where Co nucleates and grows [32]. However, the barriers which have to be overcome along this path have been found to be different. In particular, the barrier to reach the top of the discommensuration line is around twice the value for the migration barriers in hcp and fcc sites [33,34]. This could explain the repelling property of discommensuration lines with respect to diffusing Co adatoms. Finally, surface defects constitute even more efficient traps than at room temperature. These are mainly dislocations, elbows or random atomic impurities. It is worth noting that the density of the latter can be significant due to the reduced sputtering time used for this thin film sample.

As expected, if we further decrease the temperature of deposition down to 50 K ($\theta_{\text{Co}} = 0.15 \text{ ML}$), the diffusion of adatoms is completely frozen and a post nucleation regime is observed, giving rise to frozen disorder. As shown in Fig. 4d, monolayer-thick dots with lateral size of a few angstroms nucleate at spatially random locations with a high density. A rather similar phenomenon was observed on Au(111) surface with herringbone reconstruction [35].

The temperature control over diffusion barriers is an elegant way to drive the self-assembly of nanostructures, and we successfully employed it to grow elongated dots also in the present case. However in order to limit the impact of defects and achieve a more homogeneous growth, we exercised a better control on the number of nucleation centers on the surface. Pt seeding appears to be a suitable candidate to elaborate a pre-patterning of the surface [36]. Pt is miscible with Au and previous studies showed that when deposited at room temperature on Au(111), Pt substitutes Au atoms on the surface layer [37]. Since at room temperature the Au(111) surface could host a maximum of 0.03 ML of Pt, we increased the substrate temperature to 400 K to favor the exchange of Pt with Au atoms. Fig. 5a shows a room temperature STM image of 0.05 ML of Pt deposited on Au(111) at 400 K. The embedded Pt atoms are seen darker than the surrounding Au atoms, with an apparent height difference of 0.2 \AA with respect to the mean surface level. As a detrimental consequence of the alloying, Au atoms are ejected from the surface and form dots (2.35 \AA high) that may disturb the regularity of the reconstruction. More importantly, Pt atoms alloying does not occur randomly on the surface but takes place preferentially in the discommensuration regions (See inset of Fig. 5a). Thus the surface alloy could be regarded as a patterned surface in which Pt atoms constitute trapping sites that may trigger the nucleation of Co. The ability of a seed layer to guide the growth of materials that otherwise do not show any order has been shown also for Pd on $\text{Ni}_3\text{Al}(111)$ [38] or Ir on graphene/Ir(111) [39].

This is confirmed in Fig. 5b, where 0.15 ML of Co was deposited at room temperature on Au(111) seeded with Pt. Since the diffusion of adatoms is quenched by the presence of Pt atoms, Co dots nucleate with a high density in the form of monolayer dots with a mean lateral dimension of 1 nm. In the case of such small dots it has been shown

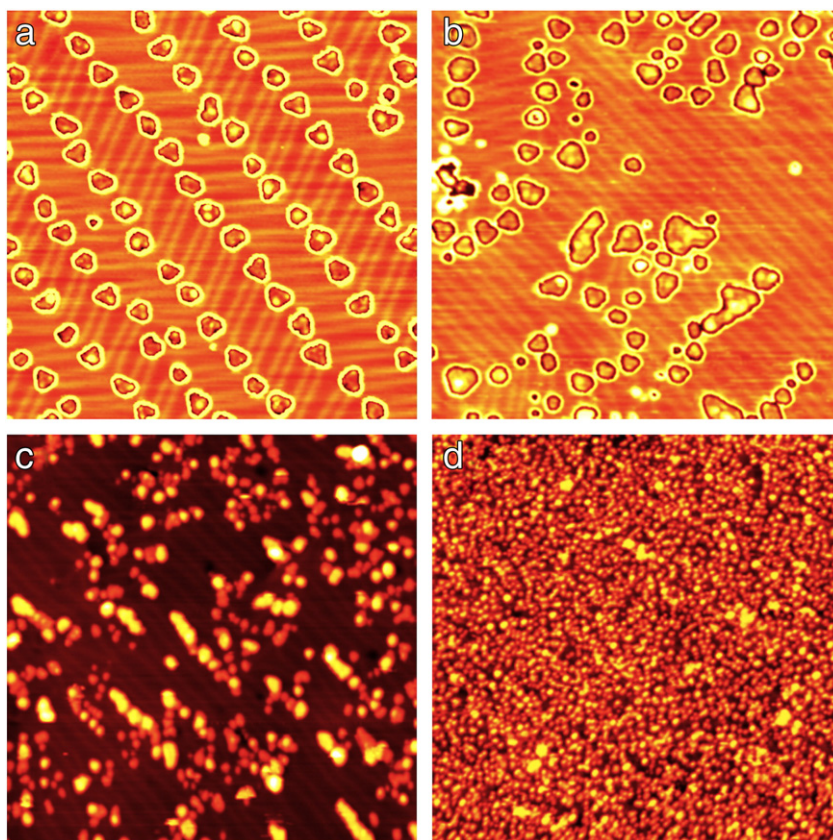


Fig. 4. STM images ($90 \times 90 \text{ nm}^2$) of Co deposited at room temperature ($\theta_{\text{Co}} = 0.25 \text{ ML}$) on Au(111) with herringbone (a) and unidirectional reconstruction (b). In both cases the images have been treated in order to enhance the contrast on the substrate. STM images of Co deposited on Au(111) with unidirectional reconstruction at low temperatures. The images are recorded at the deposition temperature. (c) $T = 105 \text{ K}$, $\theta_{\text{Co}} = 0.15 \text{ ML}$, anisotropic diffusion leads to elongated dots. (d) $T = 50 \text{ K}$, $\theta_{\text{Co}} = 0.15 \text{ ML}$, post-nucleation regime.

that it is energetically more favorable to adopt a monolayer rather than a bilayer height in order to maximize the atomic coordination [40]. The Co follows the order imposed by the previous Pt deposition and forms hemispherical dots aligned along the reconstruction lines and not on the fcc stacking regions as we observed in the low-temperature growth. In particular Co nucleates alternatively in one over two discommensuration regions and thus the distance between neighbor nanodots is 7 nm. The preferential alloying of Pt with Au takes place alternatively in one single discommensuration line of the reconstruction, as can be seen also in Fig. 5a. When θ_{Co} is increased, dots grow first vertically, adopting the usual bilayer height, and then

laterally (Fig. 5c). During this process the clusters coalesce due to the short distance between them on the same reconstruction line. As a consequence, they often form dots very elongated along the reconstruction direction, with an aspect ratio up to 8. In some other cases even if two dots come very close together, the coalescence does not take place probably due to an incommensurate growth of the dots [26]. This is observed even more systematically on Au(111) with herringbone reconstruction, and explains why the magnetic transition of Co nanodots to ferromagnetic films happen only at 1.5 ML. The problem of incommensurate growth in our case seems to be less stringent and several dots can coalesce together, as can be seen in

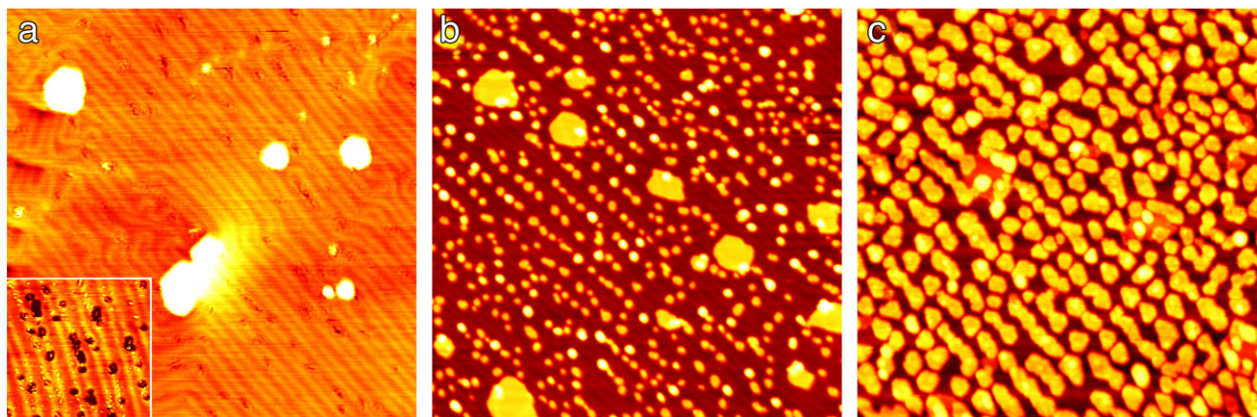


Fig. 5. (a) STM image of Pt ($\theta_{\text{Pt}} = 0.05 \text{ ML}$) deposited at 400 K on Au(111) with unidirectional reconstruction; the Pt is embedded on the surface and follows the reconstruction lines. In inset, zoom ($32 \times 32 \text{ nm}^2$) showing dark patches corresponding to Pt inserted atoms. (b) ($\theta_{\text{Co}} = 0.15 \text{ ML}$) and (c) ($\theta_{\text{Co}} = 1.1 \text{ ML}$), STM images of Co deposited on Pt/Au(111): Pt acts like preferential nucleation sites for Co that forms small and separated dots at low Co coverage (b), that coalesce when the Co coverage is increased (c). All the images are $100 \times 100 \text{ nm}^2$ and recorded at room temperature.

Fig. 5c. Another relevant difference with the Au(111) herringbone reconstruction is that the coalescence takes place in the same direction also at a macroscopic scale. Indeed, when disregarding surface defects, the direction of the reconstruction is maintained fixed. As an important consequence, the nanodots are preferentially elongated along the same axis. Significantly, this should permit macroscopically measuring the properties of such anisotropic objects along different directions. It is important to stress that no self-organized linear template with such a large period is currently available starting from nominally-flat surfaces, i.e. compatible with a standard wafer technology. This may open the way to the use of such templates for the investigation of physical properties of nanowires in a yet unexplored range of width.

4. Conclusions

In this work we employed a uniaxially strained Au(111) surface, whose reconstruction is lifted to purely linear thanks to the epitaxial constraints of an underlying multilayer sample. We investigated the capability of this surface to act as a template to obtain unidimensional nanostructures. To achieve this, we focused our attention on the growth of cobalt in submonolayer coverage. Elongated dots with an aspect ratio up to 8 were successfully obtained by following two different routes. In the first one we used the temperature to control the diffusion of adatoms across the surface. Below about 150 K the diffusion channel across the reconstruction is blocked and the anisotropic diffusion results in an elongated growth. Alternatively, we have successfully imposed ordered nucleation sites. This was done with the predeposition of a seed layer of Pt that forms a surface alloy with Au preferentially on the discommensuration lines. We believe that both these routes may be used to realize elongated nanodots of various materials (Mn, Fe, Ni, Pd, Pt....). The ability to control the diffusion and aggregation of adatoms combined with the skill to tailor a given surface structure is a powerful way to control the growth of metal nanostructures. This objective is of high importance in order to understand and exploit their physical properties.

Acknowledgment

The authors thank A. Sassella for fruitful discussions. V.R. acknowledges financial support from contract ANR-ETNAA (ANR-NANO-018-04) and Institut Universitaire de France. O.F. acknowledges financial support from contract ANR-05-NANO-073.

References

- [1] J.V. Barth, G. Costantini, K. Kern, *Nature* 437 (2005) 671.
- [2] S. Rousset, B. Croset, Y. Girard, G. Prévot, V. Repain, S. Rohart, C. R. Physique 6 (2005) 33.
- [3] J.V. Barth, H. Brune, G. Ertl, R.J. Behm, *Phys. Rev. B* 42 (1990) 9307.
- [4] H. Brune, *Surf. Sci. Rep.* 31 (1998) 121.
- [5] D.D. Chambliss, R.J. Wilson, S. Chiang, *Phys. Rev. Lett.* 66 (1991) 1721.
- [6] H.A. Dürr, S.S. Dhesi, E. Dudzik, D. Knabben, G.V. Laan, J. Goedkoop, F.U. Hillebrecht, *Phys. Rev. B* 59 (1999) R701.
- [7] Y. Nahas, V. Repain, C. Chacon, Y. Girard, J. Lagoute, G. Rodary, J. Klein, S. Rousset, H. Bulou, C. Goyhenex, *Phys. Rev. Lett.* 103 (6) (2009) 067202.
- [8] S. Rohart, P. Campiglio, V. Repain, Y. Nahas, C. Chacon, Y. Girard, J. Lagoute, A. Thiaville, S. Rousset, *Phys. Rev. Lett.* 104 (13) (2010) 137202.
- [9] P. Ohresser, N. Brookes, S. Padovani, F. Scheurer, H. Bulou, *Phys. Rev. B* 64 (2001) 104429.
- [10] H. Röder, E. Hahn, H. Brune, J.-P. Bucher, K. Kern, *Nature* 366 (1993) 141.
- [11] H. Sahaf, L. Masson, C. Léandri, B. Aufray, G.L. Lay, F. Ronci, *Appl. Phys. Lett.* 90 (2007) 263110.
- [12] P. Gambardella, M. Blanc, H. Brune, K. Kuhnke, K. Kern, *Phys. Rev. B* 61 (2000) 2254.
- [13] X.-D. Ma, D.I. Bazhanov, O. Fruchart, F. Yildiz, T. Yokoyama, M. Przybylski, V.S. Stepanyuk, W. Hergert, J. Kirschner, *Phys. Rev. Lett.* 102 (20) (2009) 205503.
- [14] T. Aste, U. Valbusa, *New J. Phys.* 7 (2005) 122.
- [15] B. Borca, O. Fruchart, P. David, A. Rousseau, C. Meyer, *Appl. Phys. Lett.* 90 (2007) 142507.
- [16] W. Lu, C. Lieber, *Nat. Mat.* 6 (2007) 841.
- [17] P. Pauzauskie, P. Yang, *Mater. Today* 9 (2006) 36.
- [18] F. Patolsky, C. Lieber, *Mater. Today* 8 (2005) 20.
- [19] A.I. Boukai, Y. Bunimovich, J. Tahir-Kheli, J. Yu, *Nature* 451 (2008) 168.
- [20] O. Schaff, A. Schmid, N. Bartelt, J. de la Figuera, R. Hwang, *Mater. Sci. Eng. A* 319 (2001) 914.
- [21] O. Fruchart, H. Tolentino, M.D. Santis, C. Goyhenex, H. Bulou, C. Clavero, M. Przybylski, J. Kirschner, to be published.
- [22] S. Padovani, I. Chado, F. Scheurer, J.P. Bucher, *Phys. Rev. B* 59 (1999) 71815.
- [23] O. Fruchart, P. Jubert, M. Eleoui, F. Cheynis, B. Borca, P. David, V. Santonacci, A. Liénard, M. Hasegawa, C. Meyer, *J. Phys. Condens. Matter* 19 (2007) 053001.
- [24] U. Harten, A. Lahee, J. Toennies, C. Wöll, *Phys. Rev. Lett.* 54 (1985) 2619.
- [25] A. Sandy, S. Mochrie, D. Zehner, K. Huang, D. Gibbs, *Phys. Rev. Lett.* 43 (1991) 4667.
- [26] O. Fruchart, G. Renaud, A. Barbier, M. Noblet, O. Ulrich, J. Deville, F. Scheurer, J. Mane-Mane, V. Repain, G. Baudot, S. Rousset, *Europhys. Lett.* 63 (2003) 275.
- [27] S. Narasimhan, D. Vanderbilt, *Phys. Rev. Lett.* 69 (1992) 1564.
- [28] J. Engbæk, J. Schiøtz, *Phys. Rev. B* 74 (2006) 195434.
- [29] O. Fruchart, A. Rousseau, D. Schmaus, A. L'Hoir, R. Haettel, L. Ortega, *Appl. Phys. Lett.* in press.
- [30] B. Voigtländer, G. Meyer, N. Amer, *Phys. Rev. B* 44 (18) (1991) 10354.
- [31] B. Fischer, H. Brune, J. Barth, A. Fricke, K. Kern, *Phys. Rev. Lett.* 82 (8) (1999) 1732.
- [32] H. Bulou, C. Massobrio, *Superlattice Microst.* 36 (2004) 305.
- [33] H. Bulou, *Superlatt. Microstr.* 44 (2008) 533.
- [34] H. Bulou, C. Massobrio, *J. Phys. Chem. C* 112 (2008) 8743.
- [35] S. Padovani, F. Scheurer, I. Chado, J. Bucher, *Phys. Rev. B* 61 (2000) 72.
- [36] Y. Nahas, V. Repain, C. Chacon, Y. Girard, S. Rousset, *Surf. Sci.* 604 (2010) 829.
- [37] M. Pedersen, S. Helveg, A. Ruban, I. Stensgaard, E. Laegsgaard, J.K. Nørskov, F. Besenbacher, *Surf. Sci.* 426 (1999) 395.
- [38] G. Hamm, C. Becker, C. Henry, *Nanotechnology* 8 (2006) 1943.
- [39] A. N'Diaye, T. Gerber, C. Busse, J. Mysliveček, J. Coraux, T. Michely, *New J. Phys.* 11 (2009) 103045.
- [40] I. Chado, C. Goyhenex, H. Bulou, J. Bucher, *Phys. Rev. B* 69 (2004) 085413.